

## Article

# Innovative Transformation and Valorisation of Red Mill Scale Waste into Ferroalloys: Carbothermic Reduction in the Presence of Alumina

Rita Khanna <sup>1,\*</sup>, Yuri Konyukhov <sup>2</sup>, Kejiang Li <sup>3</sup>, Kalidoss Jayasankar <sup>4</sup>, Nikita Maslennikov <sup>2</sup>, Dmitry Zinoveev <sup>5</sup>, Jumar Kargin <sup>6</sup>, Igor Burmistrov <sup>7</sup>, Denis Leybo <sup>8</sup>, Maksim Kravchenko <sup>9</sup> and Partha Sarathy Mukherjee <sup>10</sup>

- <sup>1</sup> School of Materials Science and Engineering (Ret.), The University of New South Wales, Sydney, NSW 2052, Australia
  - <sup>2</sup> Department of Functional Nanosystems and High-Temperature Materials, National University of Science and Technology "MISIS", 119049 Moscow, Russia; ykonukhov@misis.ru (Y.K.); masl.nik2000@gmail.com (N.M.)
  - <sup>3</sup> School of Metallurgical and Ecological Engineering, University of Science and Technology Beijing, Beijing 100083, China; likejiang@ustb.edu.cn
  - <sup>4</sup> Materials Science & Technology Division, CSIR-National Institute for Interdisciplinary Science and Technology, Thiruvananthapuram 695019, India; jayasankar@niist.res.in
  - <sup>5</sup> Laboratory of Physical Chemistry and Technology of Iron Ore Processing, A. A. Baikov Institute of Metallurgy and Materials Science, Russian Academy of Science, 119334 Moscow, Russia; dzinoveev@imet.ac.ru
  - <sup>6</sup> Technical Physics Department, Gumilev Eurasian National University, Nur-Sultan 010008, Kazakhstan; kjb\_orken@mail.ru
  - <sup>7</sup> Engineering Centre, Plekhanov Russian University of Economics, 117997 Moscow, Russia; burmistrov.in@rea.ru
  - <sup>8</sup> Laboratory of Inorganic Nanomaterials, National University of Science and Technology "MISIS", 119049 Moscow, Russia; leybo.dv@misis.ru
  - <sup>9</sup> Moscow Power Engineering Institute, National Research University, 111250 Moscow, Russia; kravchenkomv@mpei.ru
  - <sup>10</sup> Institute of Minerals and Materials Technology (Ret.), Council of Scientific and Industrial Research, Bhubaneswar 751013, India; psmukherjee52@gmail.com
- \* Correspondence: rita.khanna66@gmail.com; Tel.: +61-04-3415-5956



check for updates

**Citation:** Khanna, R.; Konyukhov, Y.; Li, K.; Jayasankar, K.; Maslennikov, N.; Zinoveev, D.; Kargin, J.; Burmistrov, I.; Leybo, D.; Kravchenko, M.; et al. Innovative Transformation and Valorisation of Red Mill Scale Waste into Ferroalloys: Carbothermic Reduction in the Presence of Alumina. *Sustainability* **2023**, *15*, 16810. <https://doi.org/10.3390/su152416810>

Academic Editors: Richard Diaz Alorro, Kazutoshi Haga and Manis Kumar Jha

Received: 2 November 2023

Revised: 2 December 2023

Accepted: 11 December 2023

Published: 13 December 2023



**Copyright:** © 2023 by the authors. Licensee MDPI, Basel, Switzerland. This article is an open access article distributed under the terms and conditions of the Creative Commons Attribution (CC BY) license (<https://creativecommons.org/licenses/by/4.0/>).

**Abstract:** Primary and secondary mill scales (MSs) are waste products produced by the surface oxidation of steel during the hot (800 to 1200 °C) rolling process in downstream steelmaking. While the primary MS is comprised of FeO, Fe<sub>3</sub>O<sub>4</sub>, and Fe<sub>2</sub>O<sub>3</sub> in a range of proportions, the secondary MS primarily contain red ferric oxide (Fe<sub>2</sub>O<sub>3</sub>) (red MS). We report a novel route for extracting iron from red MS and transforming it into ferro-aluminium alloys using carbothermic reduction in the presence of alumina. The red MS powder was blended with high-purity alumina (Al<sub>2</sub>O<sub>3</sub>) and synthetic graphite (C) in a range of proportions. The carbothermic reduction of red MS-Al<sub>2</sub>O<sub>3</sub>-C blends was carried out at 1450 °C and 1550 °C under an argon atmosphere for 30 min and then furnace-cooled. The red MS was completely reduced to iron at these temperatures with reduced iron distributed around the matrix as small droplets. However, the addition of alumina unexpectedly resulted in a significant increase in the number and sizes of iron droplets generated, much higher reactivity, and the formation of ferrous alloys. A small amount of alumina reduction into metallic aluminium was also observed at 1450 °C. There is an urgent need to identify the true potential of industrial waste and the materials within it. This study showed that red MS is a valuable material source that could be transformed into ferro-aluminium alloys. These alloys find application in a range of industrial sectors such as construction, automotive, infrastructure, etc.

**Keywords:** valorisation; ferroalloys; red mill scale waste; carbothermic reduction; construction; nanomaterials

## 1. Introduction

The iron and steelmaking industry is facing significant environmental challenges in terms of energy consumption, greenhouse gas emissions, industrial waste generation, and pollution-related issues [1]. Being one of the largest global industries, there is an urgent need to enhance the environmental sustainability of various processes within steel manufacturing. With global steel production increasing from 850 million tons (MTs) per annum in 2000 to 1879 MTs in 2021 [1], the generation of waste by-products such as slags, dust, sludges, mill scales, etc., has also seen tremendous increases. While a significant proportion of these wastes tend to be reutilised within the industry, these choices may not be the most appropriate options for material extraction. Currently, iron-bearing mill scale (MS) wastes generated during the downstream processes of hot rolling and finishing are receiving increasing attention and are the focus of this investigation.

In view of depleting natural resources and the economic and environmental costs associated with primary mining, industrial wastes could play a significant role as alternative material resources. Supplementary Figure S1 shows the distribution of average mill scale waste (in million tons (MTs); 39 MTs global total) generated in different regions of the world in 2021. China was the leading producer of mill scale waste with significant productions in other global regions as well. There is an urgent need to develop effective new techniques for valorising such industrial waste, and their commercial utilisation in various sectors. In the construction industry, steel and ferroalloys find extensive applications as structural frames, cladding, and roofing in buildings, bridges, and large structures [2]; the construction industry accounts for more than 50% global demand for steel. Other applications of ferroalloys include utilisation in the automotive sector, transport networks, infrastructure projects, utilities, pipelines, etc. Ferroalloys produced from recycling mill scale waste would find application in a wide range of industrial scenarios. A brief background on the generation, recycling of mill scales, and low-temperature carbothermic reduction of alumina is provided next.

### 1.1. Background

#### 1.1.1. Generation of Mill Scales

Mill scales are produced during the oxidation of steel surfaces during the hot rolling process for transforming semi-finished steel products into finished products. Steel strips are typically hot-rolled in the temperature range from 800 to 1200 °C. During this operation, hot steel is exposed to an oxidizing atmosphere, leading to surface oxidation in the form of primary mill scales [3–5]; the oxidation of steel and the formation of scales in this process are difficult to control and unavoidable. These mill scales are removed either mechanically or using high-pressure water, material cooling, and gravity separation [6,7]. The amounts of primary mill scales generated depend on rolling mill practices and are typically ~2% of the total steel rolled [8,9].

Even after the removal of primary scales, carbon steel is re-oxidised very quickly at elevated temperatures, so the rolling always involves steel surfaces covered with scales. This secondary scale needs to be removed completely to avoid surface defects and corrosion in the finished products and to prevent wear on the rolls. Pickling, the chemical removal of scales by immersion in an aqueous acid solution, is one of the most common processes to remove secondary scales from steel surfaces. Inorganic acids, such as hydrochloric acid, sulfuric acid, hydrofluoric acid, or a mixture of acids, have been used as pickling liquor [10–12]. Hydrochloric acid has been the preferred choice during steel production. The thickness of the scale depends mainly on the processing parameters of the hot rolling mill, mainly, the coiling temperature; the rolling process itself also has a marked influence [13]. A schematic representation of the formation of primary and secondary mill scales is shown in Figure 1.

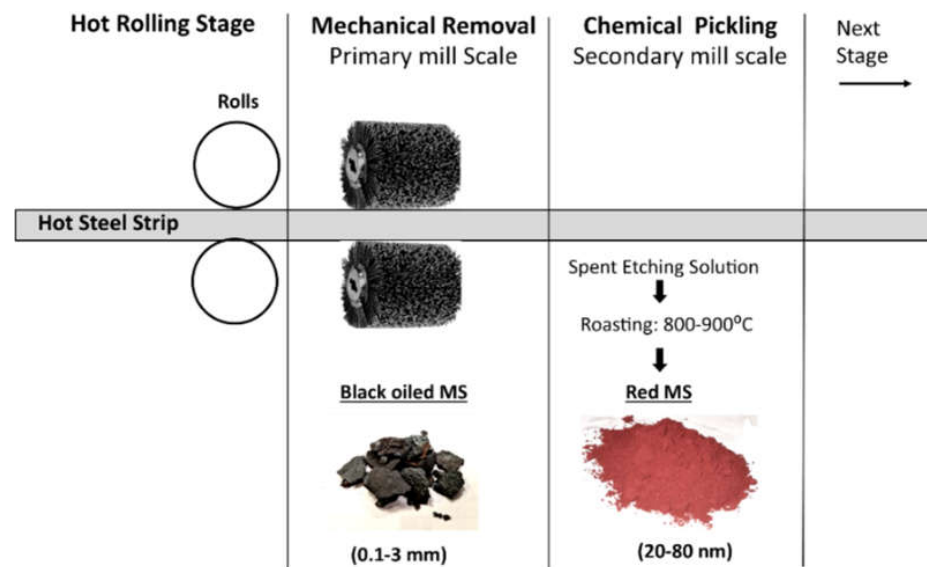


**Figure 1.** Formation of primary and secondary mill scales during the hot rolling of steel: a schematic representation.

The primary mill scale contains iron oxides in three chemical forms, namely, wüstite (mostly FeO), magnetite (Fe<sub>3</sub>O<sub>4</sub>), and hematite (Fe<sub>2</sub>O<sub>3</sub>) from the metal surface outwards; it can also contain other impurities such as C, Si, Ca, Na, Al, or Mn and other metal oxides depending on the steel being rolled. On the other hand, the secondary mill scale is primarily composed of red ferric oxide (Fe<sub>2</sub>O<sub>3</sub>) caused by the oxidation of the innermost layer of wüstite; the thickness of this secondary layer is typically less than 0.1 mm. The secondary mill scale is also referred to as the red mill scale (red MS) [14]. This layer initially protects the steel surface from atmospheric corrosion provided no breaks occur in this layer; however, this protection disappears in the presence of any surface cracks.

#### 1.1.2. Recycling of Mill Scale Waste

Being a rich source of iron, primary mill scales are utilised as iron ore sinters/pellets in ironmaking furnaces [15,16], iron powders [17–20], and briquetting [21–23], among others. In the case of secondary mill scales, ferric oxide powder dissolves into pickling liquors, generating large volumes of spent acid solutions with high iron contents [24]; the concentration of iron ions in spent hydrochloric acid can be up to 15–30% (*w/w*) [25]. Some of the extractants used include, among others, TBP (tributyl phosphate), CYC (cyclohexanone), IA (itaconic acid), OA (phosphoric acid), etc. [26]. Due to the presence of large amounts of metal and acids, pickling residue is a hazardous waste requiring strict processing to minimise environmental damage [27]. Several attempts have been made to recover acid from the pickling liquor using solvent extraction [28], evaporation and crystallisation [29], diffusion dialysis [30], and chemical precipitation to recover iron contents [31]. Solvent extraction has been used to purify, separate, and concentrate valuable metal ions in leaching liquors, spent pickling acids, and metallurgical wastes [32,33].

#### 1.1.3. Low-Temperature Carbothermic Reduction of Alumina

We first present a brief overview of the commercial production of aluminium. Aluminium is produced from the bauxite ore primarily with the electrolytic reduction of alumina using the Hall–Heroult process [34]. This process is ranked among the most energy and CO<sub>2</sub>-intensive industrial processes [35]. The direct carbothermic reduction of alumina: Al<sub>2</sub>O<sub>3</sub> + 3C = 2Al + 3CO (g), proposed as an alternative process for primary aluminium production, requires temperatures above 2100 °C and suffers from critical design issues such as aluminium carbide and oxycarbide formation, aluminium vaporisation, and low metal yields [36]. There is a pressing need to discover new ways to produce

aluminium-based products that are energy efficient, economical, and environmentally sustainable.

Based on a novel and innovative concept, our group has succeeded in lowering conventional alumina reduction temperatures (~2100–2500 °C) significantly and successfully produced ferro-aluminium alloys during carbothermic reduction in the Fe<sub>2</sub>O<sub>3</sub>-Al<sub>2</sub>O<sub>3</sub>-C system at 1550 °C [37]. Bypassing the primary production routes of both Al and Fe, this single-step approach to making ferrous alloys also results in significant reductions in energy consumption and CO<sub>2</sub> emissions [38].

### 1.2. Aim of This Investigation

In this article, we present a novel route to extract iron from the red mill scale and its transformation into ferro-aluminium alloys. Carbothermic reduction investigations were carried out on the red MS-alumina system in the temperature range 1450–1550 °C for 30 min. The small particle size of red MS (~20–80 nm) and associated large surface area is expected to provide higher reactivity as compared to standard Fe<sub>2</sub>O<sub>3</sub> powders (typically a few microns). We report detailed investigations on the carbothermic reduction of the 'red MS-Al<sub>2</sub>O<sub>3</sub>' system over a range of compositions and temperatures and the formation of ferroalloys. It is expected that the novel, efficient, and economic transformation of iron-bearing red MS waste will be a significant advance towards waste valorisation and environmental sustainability.

## 2. Materials and Methods

### 2.1. Red MS Characterisation

The red mill scale waste used in this study was obtained from the steel pickling plants of ArcelorMittal, Temirtau, Kazakhstan. Using the spray roasting process [39], the spent acid pickling solution was sprayed into a hot reaction atmosphere (800 °C) to recover solid iron oxide particles (red MS). The basic characteristics of these powders were determined as having an average particle diameter of 142 nm, a surface area of 8.79 m<sup>2</sup>/g, and a density of 5.24 g/cm<sup>3</sup>. These characteristics were determined using Brunauer–Emmett–Teller (BET) adsorption isotherms from the Quantachrome Nova 1200e (USA) surface area analyser. Additional data on BET measurements have been provided in Supplementary Table S2. A scanning electron microscopic image shown in Supplementary Figure S2 clearly shows small particle sizes of red MS. From the XRF data, the elemental composition of these powders was determined to be Fe (65.9–74.2 wt.%), O (24.8–33.6 wt.%), and Cl (0.3–0.7 wt.%) (see Supplementary Table S1), thereby indicating Fe and O as the key constituents with Cl as a minor impurity.

### 2.2. Experimental

The red MS powder was blended with high-purity alumina (Al<sub>2</sub>O<sub>3</sub>) and synthetic graphite (C) in a range of proportions. The BET surface area of Al<sub>2</sub>O<sub>3</sub> used was in the range of 13.23–48.9 m<sup>2</sup>/g. Three sets of blends were prepared: (20 g red MS + 8 g C); (20 g red MS + 10 g Al<sub>2</sub>O<sub>3</sub> + 10 g C); and (20 g red MS + 20 g Al<sub>2</sub>O<sub>3</sub> + 10 g C). This choice of blends was based on a fundamental discovery by Khanna et al. [37], wherein the reduction temperature of alumina was lowered from 2100–2500 °C to just 1550 °C in the presence of molten iron, leading to the formation of ferro-aluminium alloys. In the present study, red mill scale waste replaced Fe<sub>2</sub>O<sub>3</sub> in the above-mentioned system, and the formation of ferroalloys was investigated for a range of operating parameters. Excess amounts of carbon were used to ensure that the reductant did not become a rate-controlling factor in this investigation. All experiments were repeated at least three times to ensure reproducibility.

The carbothermic reduction of (red MS-Al<sub>2</sub>O<sub>3</sub>-C) mixtures was carried out at 1450 °C and 1550 °C for 30 min in a Carbolite TZF 17/600 tube furnace (MISIS, Moscow, Russia) [40]. The furnace was purged with pure argon gas prior to the experiments, and a continuous gas flow (2 L/m) was maintained during the heat treatments. Blended powder mixtures (20 g) were placed in a corundum crucible and loaded into the furnace. The

furnace was heated to 1450 °C (or 1550 °C) at a heating rate of 5 °C/min; the heat treatment was conducted for 30 min. The heat-treated specimens were furnace-cooled and taken out at room temperature. Detailed characterisation was carried out using analytical techniques such as Scanning Electron Microscopy (SEM)/Energy Dispersive Spectroscopy (EDS) and X-ray diffraction (XRD). SEM/EDS investigations were carried out on Tescan Vega 3 (TESCAN, Brno–Kohoutovice, Czech Republic with Oxford instruments EDS detector) with sub-micron resolution. The specimens were carbon coated prior to microscopic investigations; EDS was carried out for microscopic and elemental analysis. The XRD data were collected using a desktop X-ray diffractometer (Difrey 401, Scientific Instruments, St. Petersburg, Russia) with Cu K $\alpha$  radiation (45 KV, 40 mA) in the angular range of 10–90°, a step size of 0.1°, and a time step of 5 s.

### 3. Results

#### 3.1. Carbothermic Reduction of Red MS

The SEM results for the (20 g red MS + 8 g C) system after heat treatment for 30 min at 1450 °C and 1550 °C are shown in Figure 2. Corresponding results for elemental mapping and XRD are also included in this figure. Bright and dark regions in SEM images respectively represent reduced iron and unconsumed carbon. This aspect is clearly indicated in the elemental mapping as well. Reduced iron appears to be locally distributed at 1450 °C and spread around the matrix. The X-ray diffraction results present structural features of the heat-treated residue; diffraction peaks for carbon and BCC iron were clearly identified and were in excellent agreement with respective JCPDS files (C: 00-025-0284; Fe: 03-065-4899). At 1550 °C, the SEM and elemental mapping images indicated the spreading of iron (now molten) containing regions with a tendency for clustering. The XRD patterns remained unchanged as the temperature increased to 1550 °C.

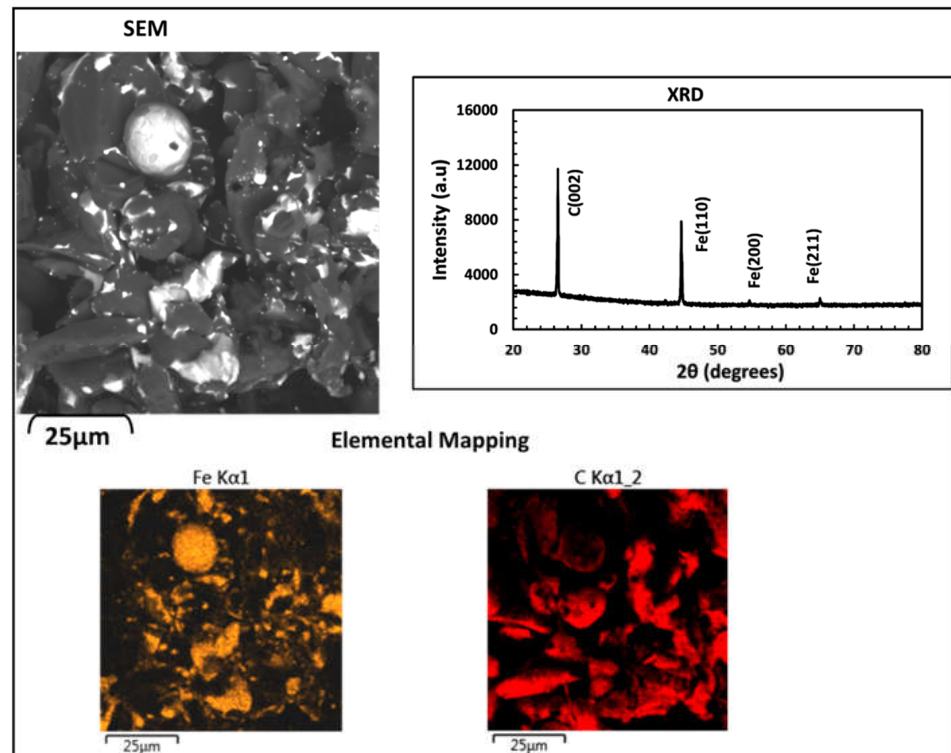
#### 3.2. Reduction Behaviour of Red MS-Al<sub>2</sub>O<sub>3</sub>-C Blends

The scanning electron microscopic results for the (20 g red MS + 10 g Al<sub>2</sub>O<sub>3</sub> + 10 g C) system, heat treated at 1450 °C for 30 min, are presented in Figure 3; these contain a high-resolution SEM image, elemental profiles, and EDS results. Bright metallic droplets are clearly seen atop the graphite chunks; several distinct regions of unreacted alumina can be seen as well. These compositional features are reflected in the corresponding elemental profiles and EDS results for points #1 and #2. A small peak of aluminium (1.1%; shown with a white arrow) was noticed at point #1. This result, which indicates the carbothermic reduction of alumina at 1450 °C, was totally unexpected. This feature will be discussed in detail in the next section.

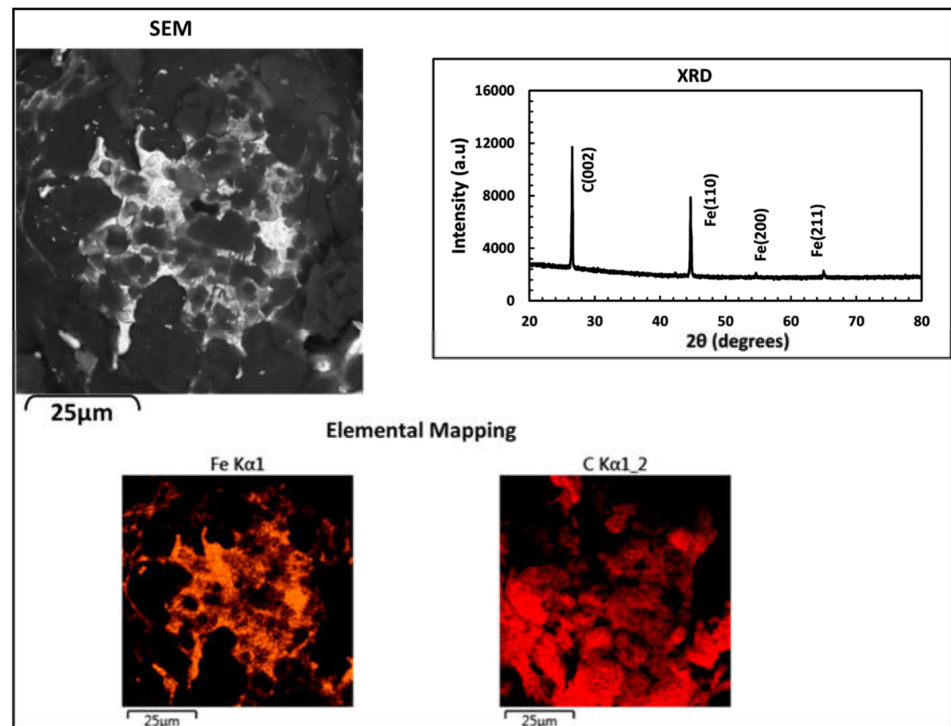
The results for the (20 g red MS + 20 g Al<sub>2</sub>O<sub>3</sub> + 10 g C) system, heat-treated at 1450 °C for 30 min, are presented in Figure 4; these also contain a high-resolution SEM image, elemental profiles, and EDS results. A small peak for aluminium can also be seen in the metallic droplet at point #1. Some regions containing unreacted alumina were seen as well.

The scanning electron microscopic results for the (20 g red MS + 10 g Al<sub>2</sub>O<sub>3</sub> + 10 g C) system, heat-treated at 1550 °C for 30 min, are presented in Figure 5; these contain a high-resolution SEM image, elemental profiles, and EDS results. Bright metallic droplets are clearly seen atop the graphite chunks. Much higher levels of Al (5.7%) were detected in the metallic droplet. The results for the (20 g red MS + 20 g Al<sub>2</sub>O<sub>3</sub> + 10 g C) heat-treated at 1550 °C are presented in Supplementary Figure S3. The amounts of Al in the metallic droplet were found to depend on the blend composition and the temperature. At 1450 °C, the amounts of Al in the (20 g red MS + 10 g Al<sub>2</sub>O<sub>3</sub> + 10 g C) and (20 g red MS + 20 g Al<sub>2</sub>O<sub>3</sub> + 10 g C) systems were 1.1% and 0.7%, respectively; the corresponding values at 1550 °C were determined to be 5.7% and 1.3%, respectively. These results indicate that the increasing proportions of Al<sub>2</sub>O<sub>3</sub> in the mix tended to reduce the amount of Al in the metallic droplet. However, the amounts of Al were found to increase with increasing temperatures.

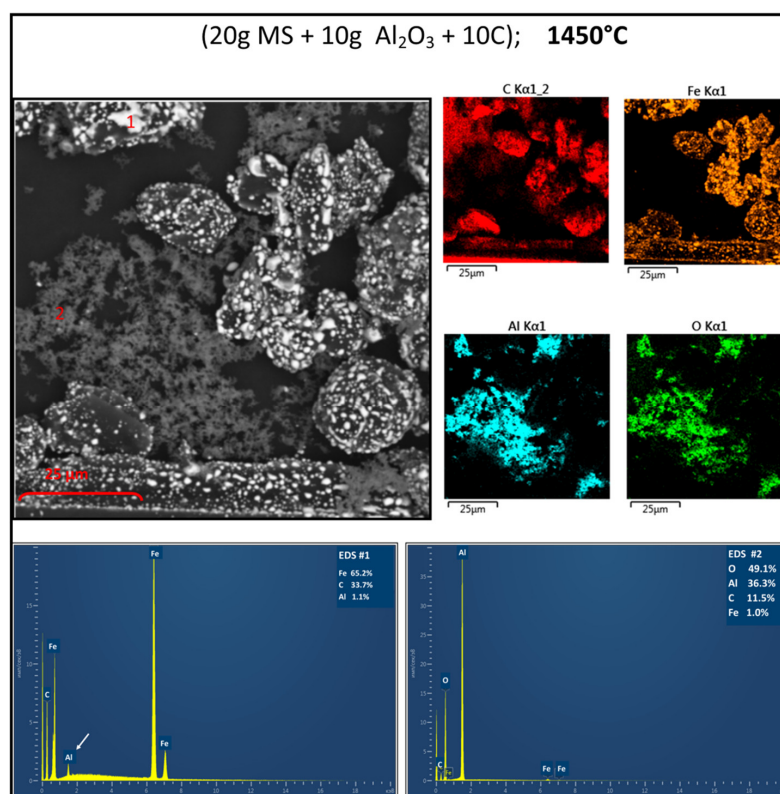
## a) 1450°C



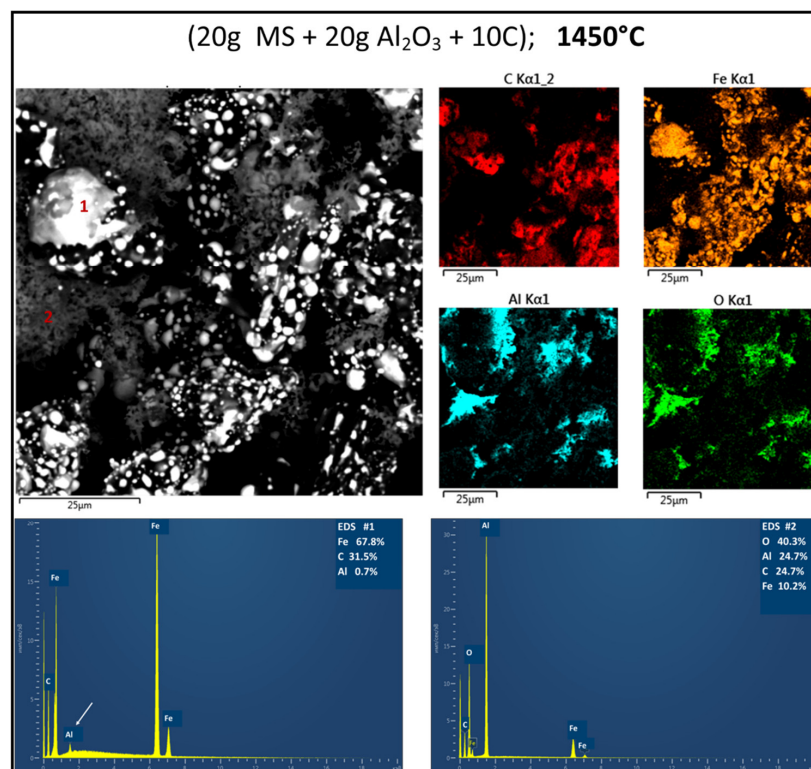
## b) 1550°C



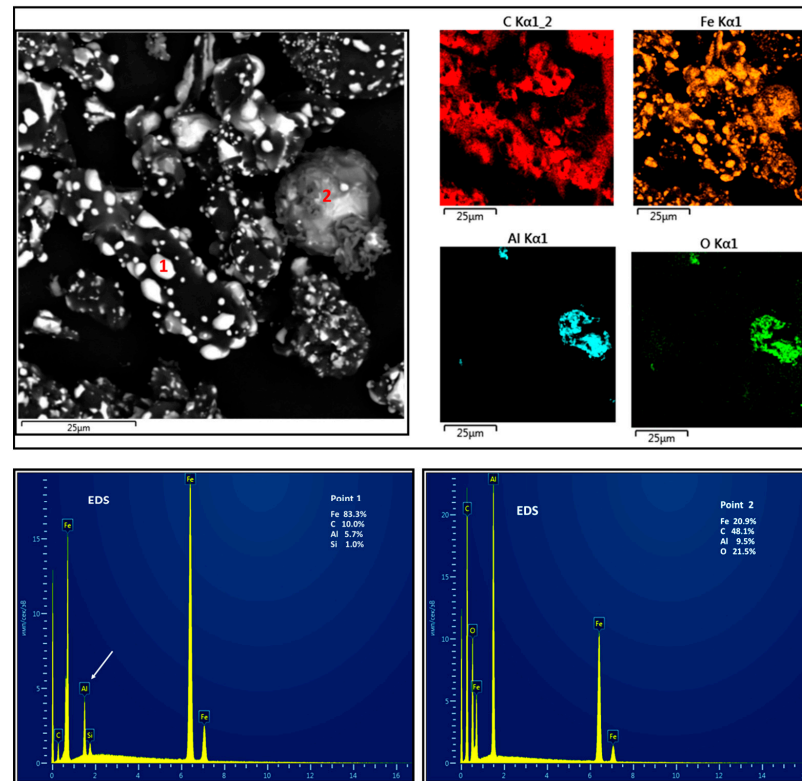
**Figure 2.** Detailed analytical results for the (20 g red MS + 8 g C) system after heat treatments at (a) 1450 °C and (b) 1550 °C for 30 min.



**Figure 3.** SEM/EDS/elemental mapping results for the (20 g red MS + 10 g Al<sub>2</sub>O<sub>3</sub> + 10 g C) system heat-treated at 1450 °C.



**Figure 4.** SEM/EDS/elemental mapping results for the (20 g red MS + 20 g Al<sub>2</sub>O<sub>3</sub> + 10 g C) system heat-treated at 1450 °C.

(20g MS + 10g Al<sub>2</sub>O<sub>3</sub> + 10C); 1550 °C

**Figure 5.** SEM/EDS/elemental mapping results for the (20 g red MS + 10 g Al<sub>2</sub>O<sub>3</sub> + 10 g C) system heat-treated at 1550 °C.

### 3.3. Structure Determination

The X-ray diffraction results for the (20 g red MS + 10 g Al<sub>2</sub>O<sub>3</sub> + 10 g C) system are presented in Figure 6; the data for both 1450 °C and 1550 °C are plotted. These measurements were carried out on the bulk powder residues. While both plots showed diffraction peaks for Al<sub>2</sub>O<sub>3</sub>, C, and metallic iron; two peaks for Fe<sub>3</sub>AlC (marked in red) were observed in the XRD patterns for 1550 °C (JCPDS files: Al<sub>2</sub>O<sub>3</sub> (00-042-1468; Fe<sub>3</sub>AlC: 04-005-5393). The peak height for 'Fe' at 1550 °C was significantly smaller compared with the corresponding peak at 1450 °C. These results clearly mark the transformation of metallic iron into Fe<sub>3</sub>AlC at 1550 °C. Although small amounts of aluminium were seen in the EDS spectra at 1450 °C, these were not reflected in the XRD patterns. Corresponding XRD results for the (20 g red MS + 20 g Al<sub>2</sub>O<sub>3</sub> + 10 g C) system are provided in Supplementary Figure S4.

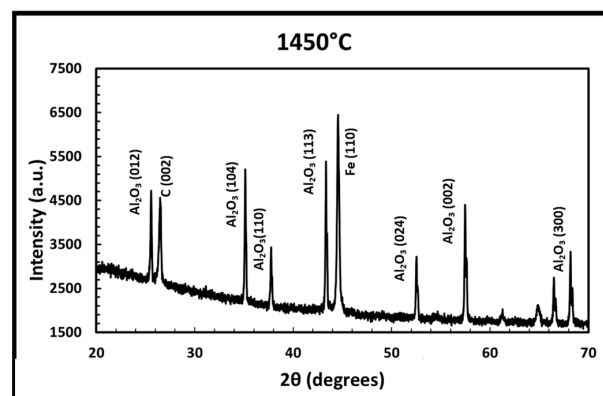


**Figure 6.** Cont.

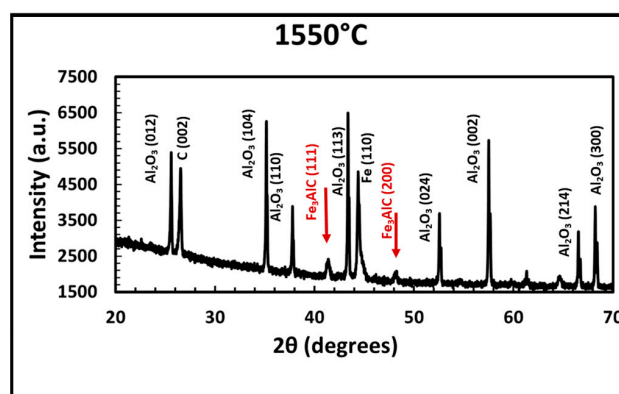


**Figure 6.** X-ray diffraction patterns for the (20 g red MS + 10 g  $\text{Al}_2\text{O}_3$  + 10 g C) system after heat treatments at 1450 °C and 1550 °C.

#### 4. Discussion

Although secondary mill scales are produced in significant quantities, research into their likely applications has been limited. There has been a tendency to dump residual iron-bearing waste acids into landfills. Landfilling such hazardous waste is undesirable as well as environmentally unsustainable, as iron-based reactions/products can generate localised heat, leachates, and gases, causing local strains and instabilities during the natural weathering of landfills [41]. Only a few studies have been reported on transforming red MS waste into nano-powders and superparamagnetic nano-adsorbents for water decontamination [42,43].

In this investigation, we presented detailed results on the carbothermic reduction of the red MS- $\text{Al}_2\text{O}_3$ -C system at 1450 °C and 1550 °C. While several of the results followed expected trends in the carbothermic reduction in the  $\text{Fe}_2\text{O}_3$ - $\text{Al}_2\text{O}_3$ -C system [37,38], there were some novel and unexpected findings as well. These aspects are discussed next.

##### 4.1. Impact on Reactivity

Due to nanosized particles and their associated high surface area, red MS was expected to be quite reactive. It was completely reduced to iron during carbothermic reduction at 1450 °C and 1550 °C for 30 min (Figure 2). The reduction of  $\text{Fe}_2\text{O}_3$  to Fe can start at temperatures above 1200 °C and become quite rapid at higher temperatures [44]; the observed reduction behaviour of red MS is therefore in accordance with well-known trends. However, there was very limited diffusion of reduced iron regions in the matrix, and these tended to be localised. Something significant occurred with the addition of alumina, a highly stable refractory oxide, to the system. A big change took place in terms of the number of iron droplets generated and their sizes. In Figure 7 (1450 °C) and Figure 8 (1550 °C), we plotted SEM images for the three blends under investigation (A: 20 g red MS + 8 g C; B: 20 g red MS + 10 g  $\text{Al}_2\text{O}_3$  + 10 g C; C: 20 g red MS + 20 g  $\text{Al}_2\text{O}_3$  + 10 g C). For ease of comparison, lower magnification (50  $\mu\text{m}$ ) SEM images were plotted in the left columns and higher magnification (5  $\mu\text{m}$ ) SEM images in the right columns of both figures. With the addition of 10 g of alumina into the blend, the numbers and sizes of iron droplets were found to increase significantly at 1450 °C, whereas there were further increases in droplet sizes at 1550 °C. With the addition of 20 g of alumina, there was little further change except the presence of unreacted alumina. Such increases in reduction reactivity were completely unexpected and were only observed for the red MS-alumina-C system. No such increases were previously reported in the carbothermic reduction reactions in the  $\text{Fe}_2\text{O}_3$ -alumina-C system [37,38]. It appears that the nano-sizes of red MS particles and their relatively higher surface area as compared with the standard micron-sized  $\text{Fe}_2\text{O}_3$  powders used in this study could play a key role in enhancing the reaction kinetics and the associated formation of ferroalloys. These results also indicate that the presence of alumina leads to much higher levels of iron extraction from the red MS.

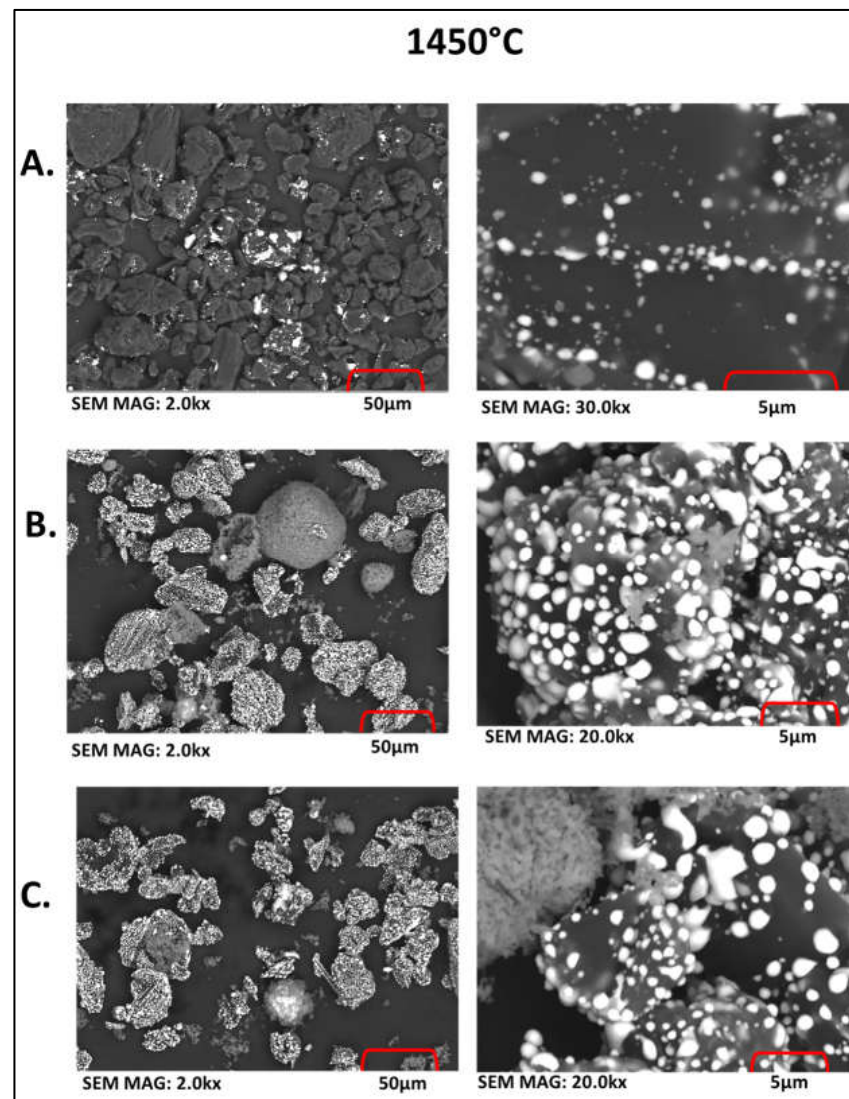


**Figure 7.** Relatively lower- (50  $\mu\text{m}$ ; left column) and higher-resolution (5  $\mu\text{m}$ ; right column) images of various blends heat-treated at 1450  $^{\circ}\text{C}$ : (A) 20 g red MS + 8 g C, (B) 20 g red MS + 10 g  $\text{Al}_2\text{O}_3$  + 10 g C, and (C) 20 g red MS + 20 g  $\text{Al}_2\text{O}_3$  + 10 g C.

#### 4.2. Lower Temperature for Alumina Reduction

In Figures 3 and 4, small amounts of “Al” were detected in the metallic droplets after the reactions of the red MS- $\text{Al}_2\text{O}_3$ -C system at 1450  $^{\circ}\text{C}$ , thereby indicating alumina reduction. This feature was not observed in previous studies on the  $\text{Fe}_2\text{O}_3$ - $\text{Al}_2\text{O}_3$ -C system [37,38]. Typically, temperatures of  $\sim 1550$   $^{\circ}\text{C}$  are required for the alumina reduction to initiate. The low-temperature carbothermic reduction of alumina takes place in a number of sequential stages [38]. These stages are:

- (1) The reduction of iron oxide and its subsequent carburisation in the molten state.
- (2) The disintegration of alumina into sub-oxide gases  $\text{AlO}$  and  $\text{Al}_2\text{O}$  ( $\text{Al}_2\text{O}_3 + \text{C} = 2\text{AlO} + \text{CO}$ ,  $\text{Al}_2\text{O}_3 + 2\text{C} = \text{Al}_2\text{O} + 2\text{CO}$ ); this reaction is known to have a slow kinetics [45].
- (3)  $\text{AlO}$  and  $\text{Al}_2\text{O}$  gases are captured by the carburised molten iron.
- (4) The subsequent reduction of these gases to Al by the solute carbon.
- (5) The dissolution of reduced Al into molten iron due to its high affinity resulted in the formation of ferro-aluminium alloys.

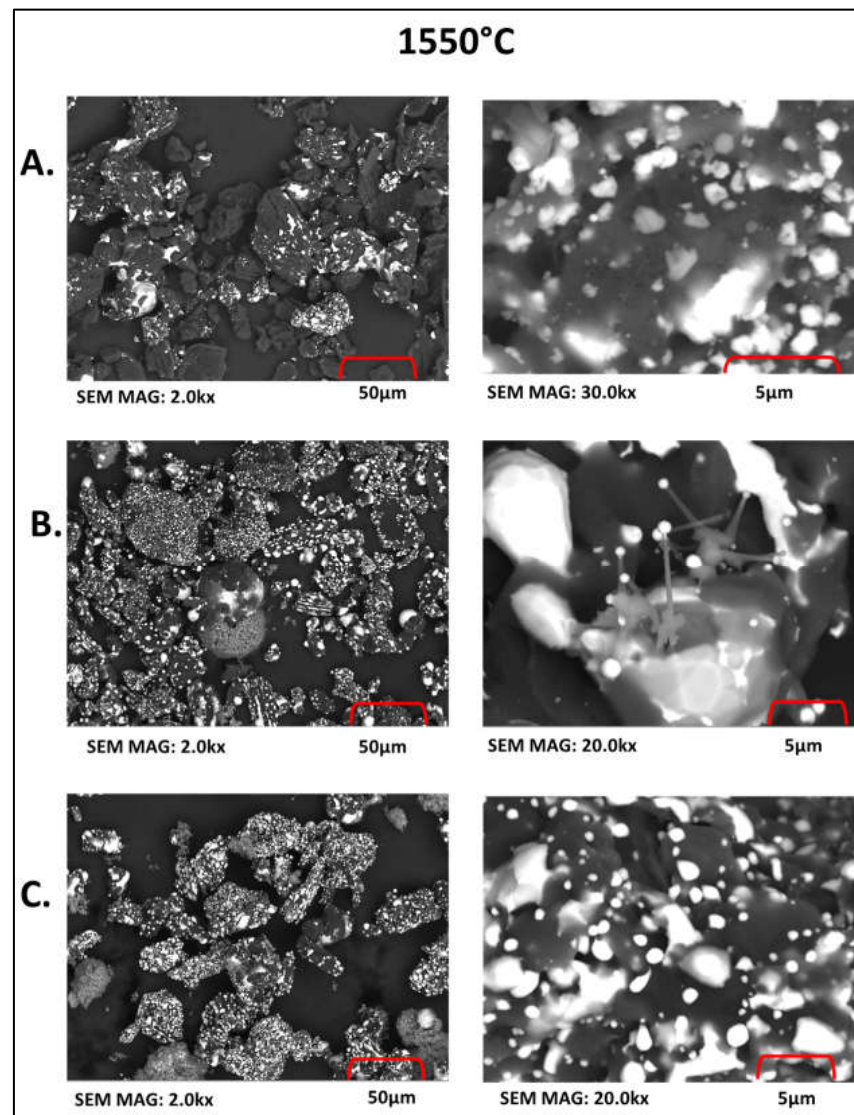


**Figure 8.** Relatively lower- (50 μm; left column) and higher-resolution (5 μm; right column) images of various blends heat-treated at 1550 °C: (A) 20 g red MS + 8 g C, (B) 20 g red MS + 10 g Al<sub>2</sub>O<sub>3</sub> + 10 g C, and (C) 20 g red MS + 20 g Al<sub>2</sub>O<sub>3</sub> + 10 g C.

A molten iron droplet was seen clearly in the SEM image at 1450 °C (Figure 3); this droplet had very high levels of carbon as well. The molten state of iron at this temperature is in good agreement with the Fe-C phase diagram [46]. The molten state of carburised iron is the key requirement for alumina reduction at low temperatures. This condition is achieved only at ~1550 °C in the case of the Fe<sub>2</sub>O<sub>3</sub>-Al<sub>2</sub>O<sub>3</sub>-C system. Khanna et al. [37] previously lowered the reduction temperature of alumina from 2100–2500 °C to 1550 °C; it appears now that these temperatures could be lowered even further to 1450 °C by replacing Fe<sub>2</sub>O<sub>3</sub> with red MS.

Among various intermetallic compounds in the binary Fe-Al phase diagram (Figure S5), both FeAl and Fe<sub>3</sub>Al have good strength and corrosion resistance and are considered very attractive for several high-temperature applications [47,48]. The formation of Fe<sub>3</sub>Al was previously reported by our group during heat treatments of the Fe<sub>2</sub>O<sub>3</sub>-Al<sub>2</sub>O<sub>3</sub>-C system at 1550 °C for 2 h [37]. In the present study on the red MS-Al<sub>2</sub>O<sub>3</sub>-C system, the heat treatments were carried out at 1450 °C and 1550 °C for 30 min only. The impact of longer heating times on the formation of Fe-Al alloys is currently being investigated at these temperatures.

Being the first study in the field, only a few process parameters and blend compositions were investigated for the extraction of iron and the formation of ferrous alloys. With several

new research directions emerging from this investigation, process optimisation will be carried out with further studies at 1400–1500 °C, heat-treatment times ranging from 10 to 180 min, alumina concentrations of 5–15 g (for 20 g red MS), and graphite concentrations of 5–10 g. Oxides other than alumina, such as SiO<sub>2</sub> or MnO<sub>2</sub>, will also be investigated.

## 5. Conclusions

1. A novel processing route was developed for extracting iron from red mill scales and its conversion to ferro-aluminium alloys. The key innovation of this study lies in blending red MS with Al<sub>2</sub>O<sub>3</sub> prior to the carbothermic reduction. The yield of iron and ferrous alloys from red MS was significantly enhanced when mixed with alumina in a range of concentrations.
2. Most studies on extracting iron from iron-bearing wastes do not use blends; instead, the waste is treated alone as a low-grade iron resource [49]. The interactions between alumina and red MS led to significant increases in reduction reactivity. This breakthrough result means that higher quantities of metal could be extracted using red MS-Al<sub>2</sub>O<sub>3</sub> blends than MS alone, leading to higher yields and significant economic benefits during waste processing.
3. This study showed that red MS could be used to prepare iron aluminides as well as Fe-Al alloys in a range of compositions. These alloys are known for their low density and good mechanical strength and can be up to 30% lighter than commercial stainless steel and other structural materials [50–52]. Iron aluminides find applications in power generation systems due to their excellent high-temperature corrosion resistance in oxidizing and sulfidizing environments [53].
4. This study showed that secondary red mill scales are a valuable material source for preparing high-value ferrous alloys. This study has the potential to open new research areas in industrial waste management wherein the use of nanosized reactants could offer significantly higher process efficiencies and productivity in a range of applications.
5. Instead of dumping industrial waste into landfills or trying to just get rid of it in any way possible, there is an urgent need to identify the true potential of the waste and the materials within it. In addition to utilising red MS waste for producing new alloys, new research directions have opened on the role of nanosized reactants in reduction reactions. It is expected that these energy-efficient waste recycling options will lead to waste valorisation and economic as well as environmentally sustainable resource utilisation and management.

**Supplementary Materials:** The following supporting information can be downloaded at: <https://www.mdpi.com/article/10.3390/su152416810/s1>. Reference [54] is cited in the Supplementary Materials.

**Author Contributions:** R.K.: conceptualisation, methodology, supervision, and writing—review and editing. Y.K.: resources, investigation, writing—original draft, and supervision. K.L.: resources and writing—review and editing. K.J.: data curation and visualisation. N.M.: methodology and investigation. D.Z.: investigation and validation. J.K.: resources and funding acquisition. I.B.: formal analysis and funding acquisition. D.L.: investigation and validation. M.K.: project administration and funding acquisition. P.S.M.: resources and formal analysis. All authors have read and agreed to the published version of the manuscript.

**Funding:** This research received no external funding.

**Institutional Review Board Statement:** Not applicable.

**Informed Consent Statement:** Not applicable.

**Data Availability Statement:** Data are contained within the article and Supplementary Materials.

**Conflicts of Interest:** The authors declare that they have no known competing financial interests or personal relationships that could have appeared to influence the work reported in this paper.

## References

1. Worldsteel Association. Environment and Climate Change. 2021. Available online: <https://worldsteel.org/steel-topics/environment-and-climate-change/> (accessed on 16 August 2023).
2. World Steel Organization. Buildings-and-Infrastructure. 2023. Available online: <https://worldsteel.org/steel-topics/steel-markets/buildings-and-infrastructure/> (accessed on 16 August 2023).
3. Basabe, V.V.; Szpunar, J.A. Growth rate and phase composition of oxide scales during hot rolling of low carbon steels. *ISIJ Int.* **2004**, *44*, 1554–1559. [[CrossRef](#)]
4. Iluțiu-Varvara, D.A.; Aciu, C.; Pică Sava, E.M. Research on the chemical characterization of the oily mill scale for natural resources conservation. *Procedia Eng.* **2017**, *18*, 439–443. [[CrossRef](#)]
5. Vlaicu, G.; Bancuta, I.; Stih, C.; Gheboianu, A.I. The study of scale formation on hot rolled ingots and billets. *J. Sci. Arts* **2010**, *12*, 161–164.
6. Khaerudini, D.S.; Chanif, I.; Insiyanda, D.R.; Destyorini, F.; Alva, S.; Pramono, A. Preparation and characterization of mill scale industrial waste reduced by biomass-based carbon. *J. Sustain. Metall.* **2019**, *5*, 510–518. [[CrossRef](#)]
7. Rieger, J.; Schenk, J. Residual processing in the European steel industry: A technological overview. *J. Sustain. Metall.* **2019**, *5*, 295–309. [[CrossRef](#)]
8. Paswan, D.; Malathi, M.; Minj, R.K.; Bandopadhyay, D. Mill scale: A potential raw material for iron and steel making. *Steel World* **2015**, *21*, 54–56.
9. Umadevi, T.; Brahmacharyulu, A.; Karthik, P.; Mahapatra, P.C.; Prabhu, M.; Ranjan, M. Recycling of steel plant mill scale via iron ore sintering plant. *Ironmak. Steelmak.* **2012**, *39*, 222–227. [[CrossRef](#)]
10. Li, L.F.; Caenen, P.; Daerden, M.; Vaes, D.; Meers, G.; Dhondt, C.; Celis, J.-P. Mechanism of single and multiple step pickling of 304 stainless steel in acid electrolytes. *Corros. Sci.* **2005**, *47*, 1307–1324. [[CrossRef](#)]
11. Lindell, D.; Pettersson, R. Pickling of process-oxidized austenitic stainless steels in HNO<sub>3</sub>-HF mixed acid. *Steel Res. Int.* **2010**, *81*, 542–551. [[CrossRef](#)]
12. Quraishi, M.A.; Rawat, J. Influence of iodide ions on inhibitive performance of Tetraphenyl-dithia-octaaza-cyclotetradeca-hexaene (PTAT) during pickling of mild steel in hot sulfuric acid. *Mater. Chem. Phys.* **2001**, *70*, 95–99. [[CrossRef](#)]
13. Pickling of Hot Rolled Strip of Carbon Steel in Pickling Lines. 2013. Available online: <https://www.ispatguru.com/pickling-of-scale-formed-on-hot-rolled-strip-of-carbon-steel/> (accessed on 15 August 2023).
14. Singh Raman, R.K. Characterisation of ‘rolled-in’, ‘fragmented’ and ‘red’ scale formation during secondary processing of steels. *Eng. Fail. Anal.* **2006**, *13*, 1044–1050. [[CrossRef](#)]
15. Eissa, M.; Ahmed, A.; El-Fawkhry, M. Conversion of Mill Scale Waste into Valuable Products via Carbothermic Reduction. *J. Metall.* **2015**, *2015*, 926028. [[CrossRef](#)]
16. Kumar, K.S.; Sah, R.; Sekhar, V.R.; Vishwanath, S.C. Development and use of mill scale briquettes in BOF. *Ironmak. Steelmak.* **2017**, *44*, 134–139. [[CrossRef](#)]
17. Martín, M.I.; López, F.A.; Torralba, J.M. Production of sponge iron powder by reduction of rolling mill scale. *Ironmak. Steelmak.* **2012**, *39*, 155–162. [[CrossRef](#)]
18. Sen, R.; Pandel, U. Closed crucible reduction of lump powdered mill scale or iron ore by coal: The sequential methodology and mechanism for optimization of process parameters. *Adv. Powder Technol.* **2020**, *31*, 3760–3773. [[CrossRef](#)]
19. Sen, R.; Maan, A.; Goyal, U.; Birdhaniya, A.; Pandel, U. In crucible reduction of mill scale by lean grade coal: Study of time, temperature and arrangement for optimum reduction conditions. *Mater. Today Proc.* **2018**, *5*, 7256–7263. [[CrossRef](#)]
20. Sista, K.S.; Dwarapudi, S.; Nerune, V.P. Direct reduction recycling of mill scale through iron powder synthesis. *ISIJ Int.* **2019**, *59*, 787–794. [[CrossRef](#)]
21. Bagatini, M.C.; Fernandes, T.; Silva, R.; Galvão, D.F.; Flores, I.V. Mill scale and flue dust briquettes as alternative burden to low height blast furnaces. *J. Clean. Prod.* **2020**, *276*, 124332. [[CrossRef](#)]
22. Jikar, P.C.; Dhokey, N.B. Influence of process parameters on counter current reactor reduction of oxidized mill scale waste and its co-relationship with mathematical model. *J. Sustain. Metall. Mater. Sci.* **2020**, *6*, 622–630. [[CrossRef](#)]
23. Zhang, Y.B.; Liu, B.B.; Xiong, L.; Li, G.H.; Jiang, T. Recycling of carbonaceous iron-bearing dusts from iron & steel plants by composite agglomeration process (CAP). *Ironmak. Steelmak.* **2017**, *44*, 532–543.
24. Su, P.; Zhang, J.; Li, Y. Chemical fixation of toxic metals in stainless steel pickling residue by Na<sub>2</sub>S·xH<sub>2</sub>O, FeSO<sub>4</sub>·6H<sub>2</sub>O and phosphoric acid for beneficial uses. *J. Environ. Sci.* **2020**, *90*, 364–374. [[CrossRef](#)]
25. Stocks, C.; Wood, J.; Guy, S. Minimization and recycling of spent acid wastes from galvanizing plants. *Resour. Conserv. Recycl.* **2005**, *44*, 153–166. [[CrossRef](#)]
26. Gao, Y.; Yue, T.; Sun, W.; He, D.; Lu, C.; Fu, X. Acid recovering and iron recycling from pickling waste acid by extraction and spray pyrolysis techniques. *J. Clean. Prod.* **2021**, *312*, 127747. [[CrossRef](#)]
27. Dahlgren, L. Treatment of Spent Pickling Acid from Stainless Steel Production: A Review of Regeneration Technologies with Focus on the Neutralization Process for Implementation in Chinese Industry. Master’s Thesis, KTH, Stockholm, Sweden, 2010.
28. Machado, R.M.; Gameiro, M.L.F.; Rodrigues, J.M.A.; Ismael, M.R.; Reis, M.T.; Carvalho, J.M. Recovery of hydrochloric acid from galvanizing industrial effluents. *Separ. Sci. Technol.* **2017**, *52*, 1333–1340. [[CrossRef](#)]
29. Leonzio, G. Recovery of metal sulphates and hydrochloric acid from spent pickling liquors. *J. Clean. Prod.* **2016**, *129*, 417–426. [[CrossRef](#)]

30. Xu, J.; Lu, S.; Fu, D. Recovery of hydrochloric acid from the waste acid solution by diffusion dialysis. *J. Hazard Mater.* **2009**, *165*, 832–837. [[CrossRef](#)]
31. Chang, Y.; Zhai, X.; Li, B.; Fu, Y. Removal of iron from acidic leach liquor of lateritic nickel ore by goethite precipitate. *Hydrometallurgy* **2010**, *101*, 84–87. [[CrossRef](#)]
32. Wang, Y.; He, Y.; Yin, S.; Long, H.; Li, S. Research on extraction of zinc from spent pickling solution using Aliquat 336. *Hydrometallurgy* **2020**, *193*, 105322. [[CrossRef](#)]
33. Mishra, R.K.; Rout, P.C.; Sarangi, K.; Nath Sarma, K.C. Solvent extraction of Fe(III) from the chloride leach liquor of low-grade iron ore tailings using Aliquat 336. *Hydrometallurgy* **2011**, *108*, 93–99. [[CrossRef](#)]
34. Calandra, A.J.; Castellano, C.E.; Ferro, C.M. The electrochemical behavior of different graphite/cryolite alumina melt interfaces under potentiodynamic perturbations. *Electrochim. Acta* **1979**, *24*, 425–437. [[CrossRef](#)]
35. European Commission. IPCC Reference Document on Best Available Techniques in the Non-ferrous Metals Industries. 2001. Available online: <http://cartuja.jrc.es/pub/english.cgi/d733223> (accessed on 16 August 2023).
36. Russell, A.S. Pitfalls and pleasures in new Aluminum process development. *Metall. Trans. B* **1981**, *12*, 203–215. [[CrossRef](#)]
37. Khanna, R.; Ikram-ul-haq, M.; Said, S.F.; Sahajwalla, V.; Mukherjee, P.S.; Seetharaman, S. Reduction reactions in Al<sub>2</sub>O<sub>3</sub>-C-Fe and Al<sub>2</sub>O<sub>3</sub>-Fe<sub>2</sub>O<sub>3</sub>-C systems at 1823K. *ISIJ Int.* **2014**, *54*, 1485–1490. [[CrossRef](#)]
38. Khanna, R.; Ikram-ul-haq, M.; Sahajwalla, V. Carbothermic reduction of alumina: On the role of molten iron and reaction mechanisms. *ISIJ Int.* **2016**, *56*, 1300–1302. [[CrossRef](#)]
39. Schiemann, M.; Wirtz, S.; Scherer, V.; Bärhold, F. Spray roasting of iron chloride FeCl<sub>2</sub>: Laboratory scale experiments and a model for numerical simulation. *Powder Technol.* **2012**, *228*, 301–308. [[CrossRef](#)]
40. Khanna, R.; Konyukhov, Y.V.; Ikram-ul-haq, M.; Burmistrov, I.; Cayumil, R.; Belov, V.A.; Rogachev, S.O.; Leybo, D.V.; Mukherjee, P.S. An innovative route for valorising iron and aluminium oxide rich industrial wastes: Recovery of multiple metals. *J. Environ. Manag.* **2021**, *295*, 113035. [[CrossRef](#)]
41. Saffarzadeh, A.; Shimaoka, T. Occurrence and significance of secondary iron-rich products in landfilled MSWI bottom ash. *Int. J. Waste Resour.* **2014**, *4*, 150.
42. Predescu, A.M.; Matei, E.; Berbecaru, A.C.; Răpă, M.; Sohaci, M.G.; Predescu, C.; Vidu, R. An innovative method of converting ferrous mill scale wastes into superparamagnetic nano adsorbents for water decontamination. *Materials* **2021**, *14*, 2539. [[CrossRef](#)]
43. Tang, J.; Pei, Y.; Hu, Q.; Pei, D.; Xu, J. The recycling of ferric salt in steel pickling liquors: Preparation of nano-sized iron oxide. *Procedia Environ. Sci.* **2016**, *31*, 778–784. [[CrossRef](#)]
44. Lundgren, M.; Khanna, R.; Ökvist, L.S.; Sahajwalla, V.; Björkman, B. The evolution of structural order as a measure of thermal history of coke in the blast furnace. *Metall. Mater. Trans. B* **2014**, *45*, 603–616. [[CrossRef](#)]
45. Frank, R.A.; Finn, C.W.; Elliott, J.F. Physical chemistry of the carbothermic reduction of alumina in the presence of a metallic solvent: Part II. Measurements of kinetics of reaction. *Metall. Trans. B* **1989**, *20*, 161–173. [[CrossRef](#)]
46. Okamoto, H. The C-Fe (Carbon-Iron) System. *J. Phase Equilib.* **1992**, *13*, 543–565. [[CrossRef](#)]
47. Murray, J.L. Fe–Al binary phase diagram. In *Alloy Phase Diagrams*; Baker, H., Ed.; ASM International: Materials Park, OH, USA, 1992; Volume 54.
48. Eggersmann, M.; Mehrer, H. Diffusion in intermetallic phases of the Fe–Al system. *Philos. Mag. A* **2000**, *80*, 1219–1244. [[CrossRef](#)]
49. Khanna, R.; Konyukhov, Y.V.; Zinoveev, D.; Jayasankar, K.; Burmistrov, I.; Kravchenko, M.; Mukherjee, P.S. Red mud as a secondary resource of low-grade iron: A global perspective. *Sustainability* **2022**, *14*, 1258. [[CrossRef](#)]
50. Deevi, S.C.; Sikka, V.K.; Liu, C.T. Processing, properties, and applications of nickel and iron aluminides. *Prog. Mater. Sci.* **1997**, *42*, 177–192. [[CrossRef](#)]
51. Liu, C.T.; George, E.P.; Maziasz, P.J.; Schneibel, J.H. Recent advances in B2 iron aluminide alloys: Deformation, fracture, and alloy design. *Mater. Sci. Eng. A* **1998**, *258*, 84–98. [[CrossRef](#)]
52. Sina, H.; Corneliusson, J.; Turba, K.; Iyengar, S. A study on the formation of iron aluminide (FeAl) from elemental powders. *J. Alloys Compd.* **2015**, *636*, 261–269. [[CrossRef](#)]
53. Tortorelli, P.F.; Natesan, K. Critical factors affecting the high-temperature corrosion performance of iron aluminides. *Mater. Sci. Eng. A* **1998**, *258*, 115–125. [[CrossRef](#)]
54. Major Steel-Producing Countries 2021 and 2020 Million Tonnes, Crude Steel Production. Available online: <https://worldsteel.org/steel-topics/statistics/world-steel-in-figures-2022/> (accessed on 25 September 2023).

**Disclaimer/Publisher’s Note:** The statements, opinions and data contained in all publications are solely those of the individual author(s) and contributor(s) and not of MDPI and/or the editor(s). MDPI and/or the editor(s) disclaim responsibility for any injury to people or property resulting from any ideas, methods, instructions or products referred to in the content.